A pseudospectral sigma-transformation model of solitary waves in a tank with uneven bed

Pseudospectral σ-Transformation Model of Solitary Waves in a Tank with Uneven Bed

Nima Vaziri[1], Ming-Jyh Chern[1,2,*], Alistair G. L. Borthwick[3]

[1] Department of Mechanical Engineering, National Taiwan University of Science and Technology, 43 Sec. 4 Keelung Road, Taipei 10607, Taiwan

[2] Center of Ecological Engineering, National Taiwan University, No. 1 Sec. 4 Roosevelt Road, Taipei 10607, Taiwan

[3]Department of Engineering Science, University of Oxford, Parks Road, Oxford OX1 3PJ, U.K.

[*] E-mail: mjchern.ntust@gmail.com; Tel: (886)-2-2737-7315; Fax: (886)-2-2737-6460

Abstract

A pseudospectral σ-transformation model is established to investigate the interaction of a solitary wave over a submerged rectangular obstacle, and an inclined bed. A piston-type wave maker is used to generate the incident solitary wave. Potential flow is assumed in the fluid domain. Close agreement is obtained between numerical predictions and previously published experimental measurements of wave interaction with the obstacle and the inclined bed. A parameter study examines the effect of obstacle height on wave evolution. The results demonstrate that the pseudospectral σ-transformation model can simulate accurately the interaction of the nonlinear solitary wave with a submerged obstacle.

Keywords: PSME method, Solitary wave, Potential flow, Submerged obstacle, Inclined bed.

1. Introduction

The interaction of waves with submerged obstacles and uneven seabed terrain is very important in certain ocean engineering problems including studies of the coastal environment, design of maritime structures, assessment of dike resilience, etc. There are many published experimental studies, analytical solutions and numerical simulations for such problems. Using linear theory, Lamb (1945) carried out the first study of wave interaction with a submerged obstacle. Later research studies included nonlinear wave models (see e.g. Rey *et al.*, 1992; Ohyama and Nadaoka, 1994 and Sue *et al.*, 2005) and detailed laboratory experiments (see e.g. Knot and Mackley, 1979). Experimental and numerical studies have also been conducted on wave propagation over an inclined bed (see e.g. Grilli *et. al.*, 1994, Madeson and Mei, 1969 and Peregrine, 1967). Useful summary reviews concerning previous studies of wave interaction with submerged obstacles are given by Huang and Dong (2001) and Sue *et al.* (2005).

The time-domain nonlinear simulation of potential flow is appropriate for the study of large amplitude waves in shallow water. In the present work, a Chebyshev pseudospectral matrix-element (PSME) method is used to solve the Laplace equation with nonlinear free surface boundary conditions for waves over an uneven bottom. This method leads to accurate, stable solutions without the need for free surface smoothing (Chern *et al.*, 1999). The PSME method is a spectral method, introduced by Ku and

Hatziavramidis (1985), used to solve many problems in fluid mechanics such as 3D incompressible fluid flow (Ku *et al.*, 1989) and free surface viscous flow (Chern *et al.*, 2005). The σ- transformation method (Philips, 1957) is used to map linearly the physical tank with uneven bed and changing free surface onto a rectangular computational domain (in a Cartesian coordinate system). The governing equation and its boundary conditions are altered accordingly to apply on the stretched grid system. The σ- transformation restricts the wave shape to be non-overturning, and so the method cannot be used for breaking or nearly breaking waves.

In our research, solitary waves are generated by a piston-like wave maker (Dong and Huang, 2004) and propagate over a submerged obstacle or an inclined bottom. The results are in good agreement with the general understanding and previous studies.

2. A Pseudospectral Matrix Element Method

The pseudospectral matrix element (PSME) method is one of the spectral methods. Consider a smooth function *u(x)* defined on the domain $x \in [-1,1]$. The Chebyshev expansion of *u* can be written in matrix notation as

$$\mathbf{u} = \mathbf{T}\hat{\mathbf{u}}, \tag{1}$$

where **T** is the matrix formed of Chebyshev polynomials and $\hat{\mathbf{u}}$ is a vector of Chebyshev coefficients. At each collocation point,

$$u_j = u(x_j) \text{ and } T_{jk} = T_k(x_j). \tag{2}$$

Collocation points, x_j, can be defined as

$$x_j = \cos(\frac{j\pi}{N}),\ j = 0,1,2,...,N. \tag{3}$$

The distribution of collocation points is located in the interval [-1, 1] and is relatively condensed at the two ends but sparse in the middle. The transformation matrix from physical space to Chebyshev spectral space is based on

$$\hat{u}_k = \frac{2}{NC_k}\sum_{j=0}^{N}\frac{1}{C_j}u(x_j)\cos\frac{\pi kj}{N},\ k = 0,1,...,N, \tag{4}$$

where

$$C_j, C_k = \begin{cases} 2 & j,k = 0,N, \\ 1 & 1 \le j,k \le N\text{-}1. \end{cases} \tag{5}$$

In matrix notation, we have

$$\hat{\mathbf{u}} = \hat{\mathbf{T}}\mathbf{u}, \tag{6}$$

where $\hat{\mathbf{T}}$ is the inverse of the matrix $\mathbf{T}$ introduced in equation (1).

Derivatives of the function u can also be transformed to Chebyshev spectral space. The qth derivative of the function u in Chebyshev spectral space can be written as

$$\frac{\mathrm{d}^q u_j}{\mathrm{d}x^q} = \sum_{k=0}^{N}\hat{u}_k^{(q)}T_k(x_j), \tag{7}$$

where the coefficients $\hat{u}_k^{(q)}$ of the derivative expansion are written in matrix notation as

$$\hat{\mathbf{u}}^{(\mathbf{q})} = \mathbf{G}^{(\mathbf{q})}\hat{\mathbf{u}}. \tag{8}$$

Equation (7) can be simplified in matrix form for practical use, i.e.

$$\frac{\mathrm{d}^{(q)}\mathbf{u}}{\mathrm{d}x^{(q)}} = \hat{\mathbf{G}}^{(\mathbf{q})}\mathbf{u}, \tag{9}$$

in which

$$\hat{\mathbf{G}}^{(\mathbf{q})} = \mathbf{T}\mathbf{G}^{(\mathbf{q})}\hat{\mathbf{T}}, \tag{10}$$

where $\mathbf{G}^{(\mathbf{q})}$ can be obtained from

$$\mathbf{G}^{(\mathbf{q})} = (\mathbf{G}^{(\mathbf{1})})^{\mathbf{q}}, \tag{11}$$

and elements of this matrix are

$$G_{ij}^{(1)} = \begin{cases} 0 & \text{if } i \geq j \text{ or } i + j \text{ even,} \\ \dfrac{2j}{C_i} & \text{otherwise.} \end{cases} \tag{12}$$

C_i is 2 at the ends and 1 at the other points. Ku and Hatziavramidis (1985) and Chern *et al.* (1999) provide more complete descriptions of this method.

3. Mathematical Model of the Solitary Wave in a Tank with an Uneven Bed

3.1. Governing Equation and Boundary Conditions in Cartesian Coordinates

Figure 1 shows a definition sketch illustrating the model domain. η is the free surface elevation above the still water level. b is the length of the tank. d is the still water depth. σ is the mapping function. The origin of the coordinate is on the mean free surface at the end of left hand side of the tank. The fluid is assumed to be inviscid and irrotational. Hence, the Laplace equation can be used as a governing equation,

$$\frac{\partial^2 \varphi}{\partial x^2} + \frac{\partial^2 \varphi}{\partial z^2} = 0, \tag{13}$$

where φ is the velocity potential function. The velocity components are zero on the boundaries (except on the wave maker side wall), i.e.

$$\frac{\partial \varphi}{\partial x} = u \text{ on } x = 0, \qquad (14)$$

where u is the horizontal velocity component of the wave maker.

$$\frac{\partial \varphi}{\partial x} = 0 \text{ on } x = b, \qquad (15)$$

and

$$\frac{\partial \varphi}{\partial z}\frac{\partial z}{\partial n} = 0 \text{ on } z = -d, \qquad (16)$$

where n is the normal direction of the bottom surface. The dynamic free surface boundary condition on $z = \eta$ is

$$\frac{\partial \varphi}{\partial t} = -g\eta - \frac{1}{2}\left[\left(\frac{\partial \varphi}{\partial x}\right)^2 + \left(\frac{\partial \varphi}{\partial z}\right)^2\right], \qquad (17)$$

where g is the acceleration due to gravity.

The kinematic free surface boundary condition can be written as

$$\frac{\partial \eta}{\partial t} = \frac{\partial \varphi}{\partial z} - \frac{\partial \varphi}{\partial x}\left(\frac{\partial \eta}{\partial x} + \frac{\partial d}{\partial x}\right). \qquad (18)$$

3.2. The σ- transformation

The above problem involves a pair of nonlinear free surface conditions, Eqs. (17) and (18), which are applied to an unknown parameter $\eta(x, t)$ at $t > 0$. Herein, this difficulty is

overcome by transforming the physical domain onto a rectangular region, using the so-called σ- transformation. The mapping function is defined as (see Figure 2 (a))

$$\sigma = -1 + \frac{2(z+d)}{h}, \tag{19}$$

where

$$h(x,t) = \eta(x,t) + d(x). \tag{20}$$

It is obvious that for $z = \eta$ and $z = -d$, the values of σ are 1 and -1, respectively. The other main transformation equations are

$$\begin{aligned} X &= -1 + \frac{2x}{b}, \\ T &= t. \end{aligned} \tag{21}$$

Using Eqs (19) and (21), the velocity potential $\varphi(x,z,t)$ can be transformed from the physical domain onto $\Phi(X,\sigma,T)$. Now the first derivatives of φ with respect to other parameters are written as

$$\begin{aligned} \frac{\partial \varphi}{\partial x} &= \frac{2}{b}\frac{\partial \Phi}{\partial X} + \left[(\frac{2}{b})(\frac{2}{h})(\frac{\partial d}{\partial X}) - (\frac{2}{b})(\frac{\sigma+1}{h})(\frac{\partial \eta}{\partial X} + \frac{\partial d}{\partial X}) \right] \frac{\partial \Phi}{\partial \sigma}, \\ \frac{\partial \varphi}{\partial z} &= (\frac{2}{h})\frac{\partial \Phi}{\partial \sigma}, \\ \frac{\partial \varphi}{\partial t} &= \left[-(\frac{\sigma+1}{h})(\frac{\partial \eta}{\partial T}) \right] \frac{\partial \Phi}{\partial \sigma} + \frac{\partial \Phi}{\partial T}. \end{aligned} \tag{22}$$

The second derivatives of φ are similarly derived by the chain rule. Finally the transformed governing equation and boundary conditions can be obtained. The transformed Laplace equation is

$$
\begin{aligned}
&(\frac{2}{b})^2\frac{\partial^2\Phi}{\partial X^2}+\left[(2)(\frac{2}{b})^2(\frac{2}{h})(\frac{\partial d}{\partial X})-(2)(\frac{2}{b})^2(\frac{\sigma+1}{h})(\frac{\partial\eta}{\partial X}+\frac{\partial d}{\partial X})\right]\frac{\partial^2\Phi}{\partial\sigma\partial X}\\
&+\left[(-2)(\frac{2}{b})^2(\frac{2}{h^2})(\frac{\partial d}{\partial X})(\frac{\partial\eta}{\partial X}+\frac{\partial d}{\partial X})+(\frac{2}{b})^2(\frac{2}{h})(\frac{\partial^2 d}{\partial X^2})+(\frac{2}{b})^2(\frac{2(\sigma+1)}{h^2})(\frac{\partial\eta}{\partial X}+\frac{\partial d}{\partial X})^2\right.\\
&-(\frac{2}{b})^2(\frac{\sigma+1}{h})(\frac{\partial^2\eta}{\partial X^2}+\frac{\partial^2 d}{\partial X^2})-(\frac{2}{b})^2(\frac{1}{h})(\frac{2}{h})(\frac{\partial d}{\partial X})(\frac{\partial\eta}{\partial X}+\frac{\partial d}{\partial X})+\\
&\left.(\frac{2}{b})^2(\frac{1}{h})(\frac{\sigma+1}{h})(\frac{\partial\eta}{\partial X}+\frac{\partial d}{\partial X})^2\right]\frac{\partial\Phi}{\partial\sigma}+\left[(\frac{2}{b})^2(\frac{2}{h})^2(\frac{\partial d}{\partial X})^2-\right.\\
&\left.(2)(\frac{2}{b})^2(\frac{2}{h})(\frac{\partial d}{\partial X})(\frac{\sigma+1}{h})(\frac{\partial\eta}{\partial X}+\frac{\partial d}{\partial X})+(\frac{2}{b})^2(\frac{\sigma+1}{h})^2(\frac{\partial\eta}{\partial X}+\frac{\partial d}{\partial X})^2+(\frac{2}{h})\right]\frac{\partial^2\Phi}{\partial\sigma^2}=0.
\end{aligned}
\tag{23}
$$

The transformed dynamic free surface boundary condition is

$$
\begin{aligned}
&\frac{\partial\Phi}{\partial T}=\left[(\frac{\sigma+1}{h})(\frac{\partial\eta}{\partial T})\right]\frac{\partial\Phi}{\partial\sigma}-g\eta-\frac{1}{2}\left[\left((\frac{2}{b})(\frac{\partial\Phi}{\partial X})+\left[(\frac{2}{b})(\frac{2}{h})(\frac{\partial d}{\partial X})-\right.\right.\right.\\
&\left.\left.\left.(\frac{2}{b})(\frac{\sigma+1}{h})(\frac{\partial\eta}{\partial X}+\frac{\partial d}{\partial X})\right]\frac{\partial\Phi}{\partial\sigma}\right)^2+(\frac{2}{h}\frac{\partial\Phi}{\partial\sigma})^2\right],
\end{aligned}
\tag{24}
$$

and the transformed kinematic free surface boundary condition is

$$
\begin{aligned}
&\frac{\partial\eta}{\partial T}=\left[(\frac{2}{h})+(\frac{2}{b})^2(\frac{2}{h})(\frac{\partial d}{\partial X})(\frac{\partial\eta}{\partial X})-\right.\\
&\left.(\frac{2}{b})^2(\frac{\sigma+1}{h})(\frac{\partial\eta}{\partial X}+\frac{\partial d}{\partial X})(\frac{\partial\eta}{\partial X})\right](\frac{\partial\Phi}{\partial\sigma})-(\frac{2}{b})^2(\frac{\partial\eta}{\partial X})\frac{\partial\Phi}{\partial X}.
\end{aligned}
\tag{25}
$$

3.3. Solitary Wave Generation

In this model, the incident solitary wave is generated using a numerical piston-type wave maker. To generate a solitary wave, one of the side walls (in this study, the right one) can move like a piston. The total displacement of the wall plate is *X(t)* and the velocity of the plate is given by (Goring and Raichlen, 1980),

$$u = \frac{\mathrm{d}X}{\mathrm{d}t} = \frac{1}{d+\eta} c\eta \,. \tag{26}$$

For a solitary wave, the water surface elevation can be expressed as (Huang and Dong, 2001)

$$\eta = a\,\mathrm{sech}^2\left[K\left(X - ct\right)\right], \tag{27}$$

where

$$K = \sqrt{3a/4d^3}\,, \tag{28}$$

and the phase velocity of the solitary wave is

$$c = \sqrt{g(a+d)}\,. \tag{29}$$

In above equations, a is the amplitude of the solitary wave, d is the still water depth and g is the acceleration of gravity. Submitting these expressions into equation (26) gives

$$\frac{\mathrm{d}X}{\mathrm{d}t} = ca\,\mathrm{sech}^2\left[K\left(X - ct\right)\right] / \left(d + a\,\mathrm{sech}^2\left[K\left(X - ct\right)\right]\right). \tag{30}$$

This equation shows the velocity of the wave maker. More details about this method can be found in Huang and Dong (2001) and Dong and Huang (2004).

3.4. Pseudospectral Discretization of Free Surface Wave Equations

Now the PSME method can be used to solve the initial boundary value problem in the transformed domain. The computational domain is defined as $-1 \le X \le 1$ and $-1 \le \sigma \le 1$. N and M are the number of collocation points in the X and σ directions, respectively. The governing equation for Φ_{ij} $(1 \le i \le N-1, 1 \le j \le M-1)$ is given by Eq. (23).

However, for all the position derivation terms in all the equations, the PSME method is applied (such that $\frac{\partial^2 \Phi}{\partial \sigma^2} = \sum_{m=0}^{M} \hat{\boldsymbol{G}}\boldsymbol{\sigma}_{jm}^{(2)} \Phi_{im}$ and $\frac{\partial^2 \Phi}{\partial X^2} = \sum_{n=0}^{N} \hat{\boldsymbol{G}}\boldsymbol{X}_{in}^{(2)} \Phi_{nj}$ where $\hat{\boldsymbol{G}}\boldsymbol{\sigma}_{jm}^{(2)}$ and $\hat{\boldsymbol{G}}\boldsymbol{X}_{in}^{(2)}$ are Chebyshev matrix coefficients in σ and X directions, respectively).

For dynamic and kinematic free surface boundary conditions, the Adams-Bashforth scheme is used to calculate the wave elevation and velocity potential. At each time step, several algebraic equations are solved to find Φ at each collocation point and also the free surface elevation of the wave. The matrix of equations is solved by successive over relaxation.

4. Numerical Results and Discussion

4.1. Model Validation

Figure 2 shows a schematic diagram of a solitary wave passing over a submerged obstacle, and a typical σ-transformed spectral mesh plotted in the physical domain (100×10 grid).

To quantitatively verify the present model, one of the cases from Seabra-Santos *et al.* (1987) is considered where a solitary wave passes over an isolated triangular obstacle. In that case, the tank of length 20 m contains water of mean depth 25 cm. The height of the obstacle is 10 cm and its base length is 14.1 cm. The initial wave elevation is 10 cm. Measurement points are located 5 cm in front of and behind the obstacle. Computations on 100×10 and 200×20 grids gave almost the same results, demonstrating grid

independence (see *e.g.* Chern *et al.*, 1999). By comparing results for different non-dimensional time steps, $\Delta t^* = \Delta t \sqrt{(g/d)} = 0.005$, 0.01, 0.02 and 0.05, (on a 100×10 grid), it is found that the program gave stable, accurate predictions provided the nondimensional time step is less than 0.01. Figures 3 and 4 present time histories of wave elevation at the measurement locations behind and in front of the submerged obstacles. The solid and dashed lines refer respectively to the present numerical predictions and the experimental data from Seabra-Santos *et al.* (1987). It can be seen that the numerical predictions are in very satisfactory agreement with the experimental data, except for the over-prediction of the solitary wave crest elevation, which may be due to frictional effects from the tank wall and bed, which are not included in the potential theory model. This case (with 100×10 grid points and $\Delta t^* = 0.01$) has been computed on a workstation with two 3.40 GHz CPU processors and 3 GB RAM memory. The CPU time required is less than 3 h.

4.2. Solitary Wave over a Submerged Rectangular Obstacle

First, a tank with still water depth to length ratio of $d/b = 1/250$ is considered. An obstacle of height $0.9d$ and length 20 cm is located at the centre of the tank. The incident solitary wave is generated by the piston-type wave maker imposed in the domain, and has an amplitude equal to $0.0055d$. Figure 5 is an x-t plot depicting the wave profile evolution between 2 and 4 seconds, after the wave has first been generated. On meeting the obstacle, the solitary wave partly splits into two transmitted waves followed by a small train of dispersive waves. Wave reflection also occurs as the incident solitary wave interacts with the submerged step.

Next, we study the effect of obstacle height on a solitary wave in shallow water. In this case, the ratio of still water depth d to the length of the tank b is d/b = 1/100, and the initial solitary wave amplitude is 0.19d. An obstacle of length of 4.5 cm is located 50 cm in front of the wave maker. The height of the obstacle varies between 0.25d and 0.90d. Figures 6 and 7 present the time histories of wave elevation for various obstacle heights at locations 10d in front of the obstacle, and 10.5d behind it, respectively. As would be expected, the amplitude of the dispersive waves increases as the height of the obstacle increases. The effect of a very tall obstacle (d_o=0.90d) on the solitary wave before obstacle is significant. In addition, the timing of the maximum crest elevation of the solitary wave along the tank is influenced slightly by the relative height of the submerged obstacle, as can be seen by the phase shift in Figure 7.

4.3. Solitary Wave over an Inclined Bottom

The final case considers the effect of inclined bottom on the propagation of a solitary wave. Figure 8 defines the geometry of the problem, whereby an incident solitary wave travels over a flat bed, then over an inclined bed of slope, α, onto a shelf. The solitary wave elevations before and on the shelf are denoted η_o and η; similarly, the water depths before and on the shelf are denoted d_o and d. In the numerical simulation, d_o = 1 and d = 0.4, the beach slope is 1/20 and the initial value of solitary wave elevation before the shelf is 0.1d_o. Figure 9 shows the predicted variation in relative wave elevation (η/η_o) with the relative depth (d/d_o), and also includes Peregrine's (1967) experimental data.

The predictions show the same trend as Peregrine's experimental results, but the values are generally under-estimated (except for low values of d/d_o). For $d=0.5d_o$, the error is about 3%. The reason for this difference is likely to be due to the inviscid, frictionless flow assumptions inherent in potential theory, which means that viscous turbulent effects are neglected along with bed and sidewall friction. It was also observed from the evolution of the wave profiles with time (not plotted here to save space) that the shape of the solitary wave became distorted as it travelled up the slope, the wave crest became more peaked as the maximum amplitude increased with decreasing water depth on the shelf, and the main solitary wave shed a dispersive wave.

5. Conclusions

A pseudospectral σ-transformation model to simulate a solitary wave motions has been established, and used to investigate the interactions of solitary waves with a submerged obstacle and an inclined bed. It has been demonstrated that the PSME method is capable of simulating the behaviour of solitary waves over an uneven bed, bearing in mind the limitations of potential theory which neglects rotationality, viscous effects, turbulence, and friction. For solitary waves passing over a submerged obstacle, the numerical predictions show that dispersive wave elevation increases as the relative height of the obstacle to the water depth increases. For solitary waves propagating over an inclined bed and onto a shelf, the solitary wave elevation increases as the water depth decreases, as would be expected. The results are in reasonable agreement with previously published experimental data.

Acknowledgment – The first author is grateful to the National Science Council of Taiwan for its generous financial support (NSC 99-2221-E-011-041).

References

1. Chern, M.J., Borthwick, A.G.L., Eatock Taylor, R., 1999. A pseudospectral σ-transformation model of 2-d nonlinear waves. *Journal of Fluids and Structures*. **13**(5), 607-630.

2. Chern, M.J., Borthwick, A.G.L., Eatock Taylor, R., 2005. Pseudospectral element model for free surface viscous flows. *International Journal for Numerical Methods for Heat and Fluid Flow*. **15**(6), 517-554.

3. Dong, C.M., Huang, C.J., 2004. Generation and propagation of water waves in a two-dimensional numerical viscous wave flume. *ASCE J. Waterway, Port, Coastal, and Ocean Engineering*. **130**(3), 143-153.

4. Grilli, S.T., Subramanya, R., Svendsen, I.A., Veeramony, J., 1994. *ASCE J. Waterway, Port, Coastal, and Ocean Engineering*. **120**(6), 609-628.

5. Goring, D.G., Raichlen, F., 1990. Propagation of long waves onto shelf. *ASCE J. Waterway, Port, Coastal, and Ocean Engineering*. **118**, 43–61.

6. Huang, C.J., Dong, C.M., 2001. On the interaction of a solitary wave and a submerged dike. *Coastal Engineering*. **43**, 265–286.

7. Knott, G.F., Mackley, M.R., 1980. On eddy motions near plates and ducts, induced by water waves and periodic flows. *Phil. Trans. Roy. Soc. (Lond.) A*. **A294**(1412), 559–623.

8. Ku, H.C., Hatziavramidis, D., 1985. Solutions of the 2 dimensional Navier-Stokes equations by Chebyshev expansion methods. *Computers and Fluids*. **13**(1), 99-113.

9. Lamb, H., 1945. *Hydrodynamics*. 6th Edition, Cambridge University Press, England.

10. Madsen, O.S., Mei, C.C., 1969. The transformation of a solitary wave over an uneven bottom. *Journal of Fluid Mechanics*. 39, 781-791.

11. Ohyama, T., Nadaoka, K., 1994. Transformation of a nonlinear wave train passing over a submerged shelf without breaking. *Coastal Engineering*. **24**, 1–22.

12. Peregrine, D.H., 1967. Long waves on a beach. *Journal of Fluid Mechanics*. 27, 815-827.

13. Phillips, N.A., 1957. A coordinate system having some special advantages for numerical forecasting. *Journal of Meteorology*. **14**(2), 184-185.

14. Rey, V., Belzons, M., Guazzelli, E., 1992. Propagation of surface gravity waves over a rectangular submerged bar. *Journal of Fluid Mechanics*. **235**, 453–479.

15. Seabra-Santos, F.J., Renouard, D.P., Temperville, A.M., 1987. Numerical and experimental study of the transformation of a solitary wave over a shelf or isolated obstacle. *Journal of Fluid Mechanics*. **176**, 117-134.

16. Sue, Y.C., Chern, M.J., Hwang, R.R., 2005. Interaction of nonlinear progressive viscous waves with a submerged obstacle. *Ocean Engineering*. **32**(8-9), 893–923.

List of Figures

Fig. 1 Definition sketch of uneven bed tank model.

Fig. 2 (a) Schematic diagram of a solitary wave passing over a submerged obstacle. (b) A typical σ-transformed spectral mesh plotted in the physical domain. The free surface profile is exaggerated (by scaling the vertical dimension by 500).

Fig. 3 Validation case of solitary wave interaction with a submerged triangular obstacle: wave elevation time history at a location 5 cm behind the obstacle (solid line = present numerical predictions; dashed line = experimental data from Seabra-Santos *et al.* (1987)).

Fig. 4 Validation case of solitary wave interaction with a submerged triangular obstacle: wave elevation time history at a location 5 cm in front of the obstacle (solid line = present numerical predictions; dashed line = experimental data from Seabra-Santos *et al.* (1987)).

Fig. 5 Evolution of solitary wave as it interacts with a submerged rectangular obstacle: *x-t* plots of wave profile at prescribed time intervals.

Fig. 6 Wave elevation time histories at $x/d = 10$ before the obstacle, for solitary waves of different initial amplitudes.

Fig. 7 Wave elevation time histories at $x/d = 10.5$ after the obstacle, for solitary waves of different initial amplitudes.

Fig. 8 Definition sketch of solitary wave passing over an inclined bed onto a shelf.

Fig. 9 Non-dimensional amplitude variation with depth, for beach slope=1/20 (solid line = present study; open circles = experimental data from Peregrine (1967)).

Figures

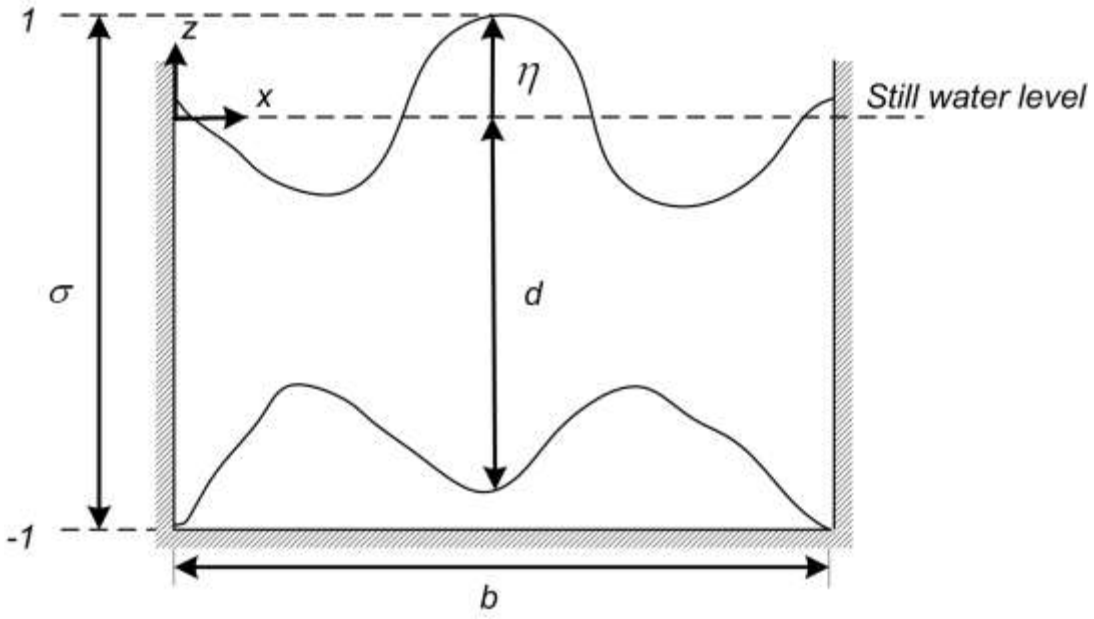

Fig. 1 Definition sketch of uneven bed tank model.

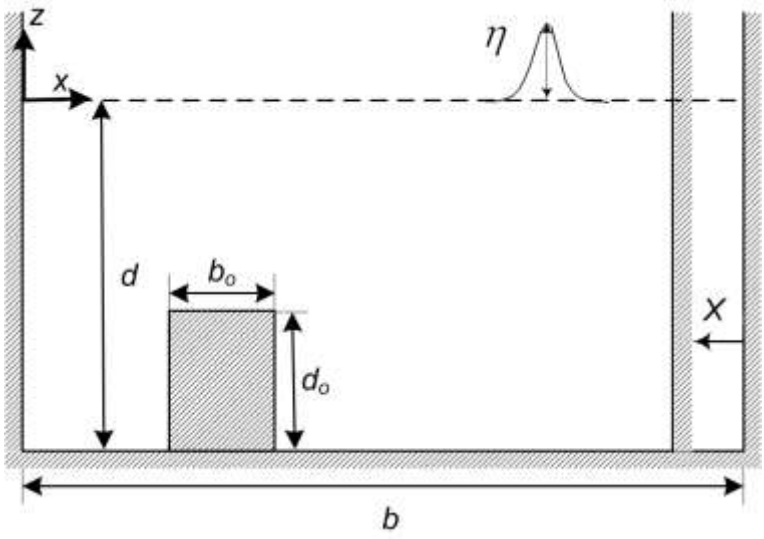

Fig. 2 (a) Schematic diagram of a solitary wave passing over a submerged obstacle.

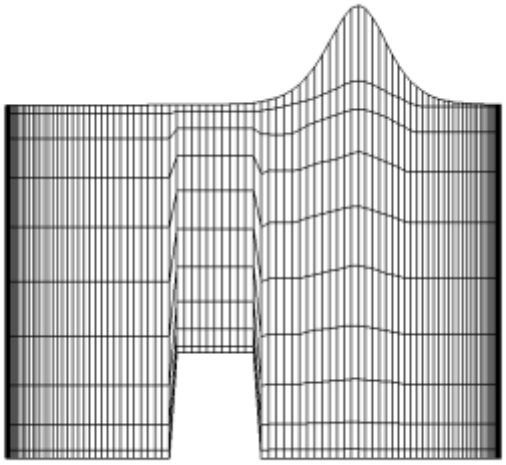

Fig. 2 (b) A typical σ-transformed spectral mesh plotted in the physical domain. The free surface profile is exaggerated (by scaling the vertical dimension by 500).

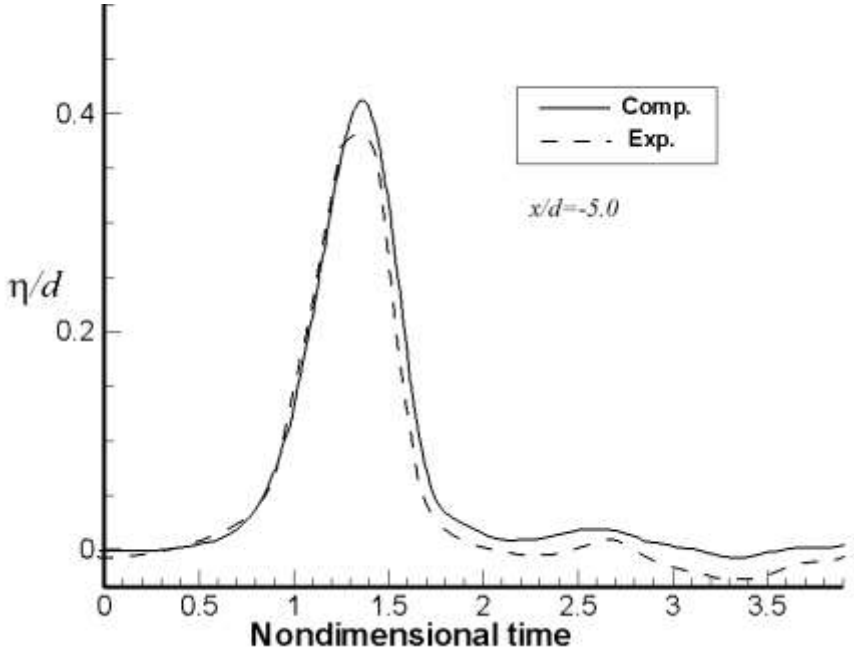

Fig. 3 Validation case of solitary wave interaction with a submerged triangular obstacle: wave elevation time history at a location 5 cm behind the obstacle (solid line = present numerical predictions; dashed line = experimental data from Seabra-Santos *et al.* (1987)).

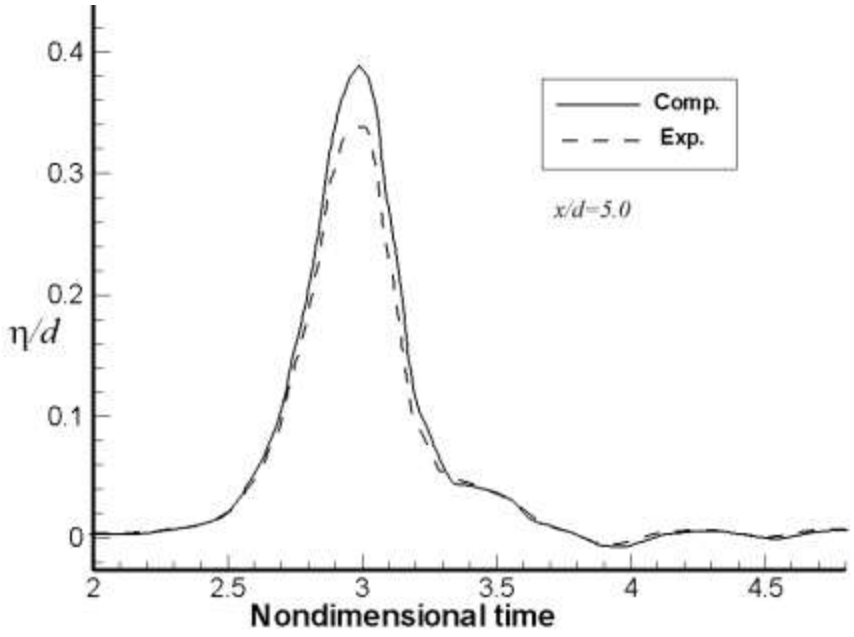

Fig. 4 Validation case of solitary wave interaction with a submerged triangular obstacle: wave elevation time history at a location 5 cm in front of the obstacle (solid line = present numerical predictions; dashed line = experimental data from Seabra-Santos *et al.* (1987)).

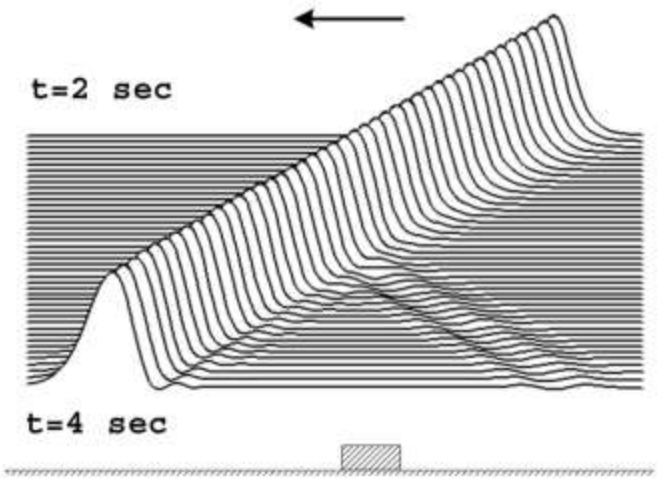

Fig. 5 Evolution of solitary wave as it interacts with a submerged rectangular obstacle: *x-t* plots of wave profile at prescribed time intervals.

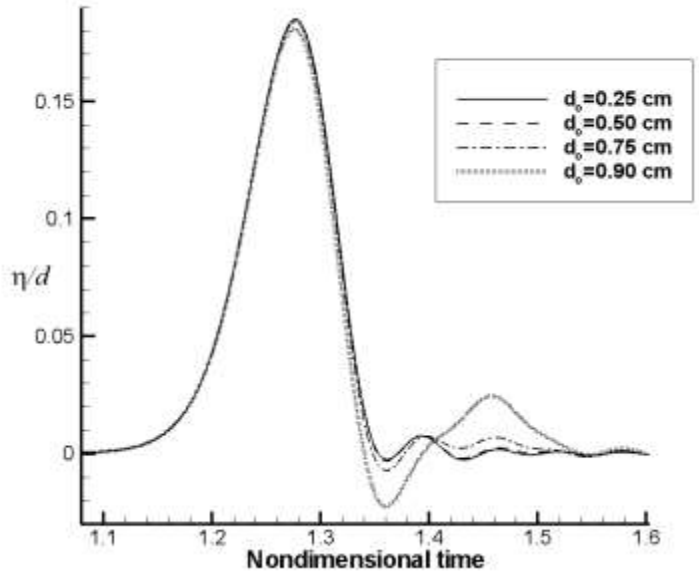

Fig. 6 Wave elevation time histories at $x/d = 10$ before the obstacle, for solitary waves of different initial amplitudes.

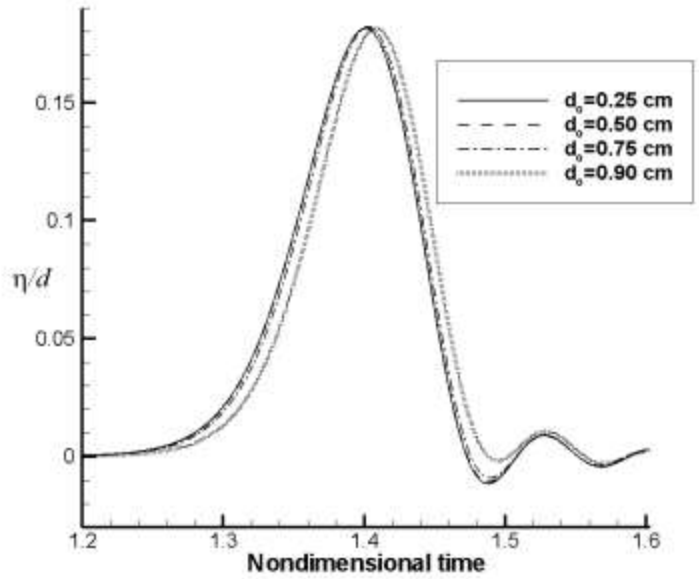

Fig. 7 Wave elevation time histories at $x/d = 10.5$ after the obstacle, for solitary waves of different initial amplitudes.

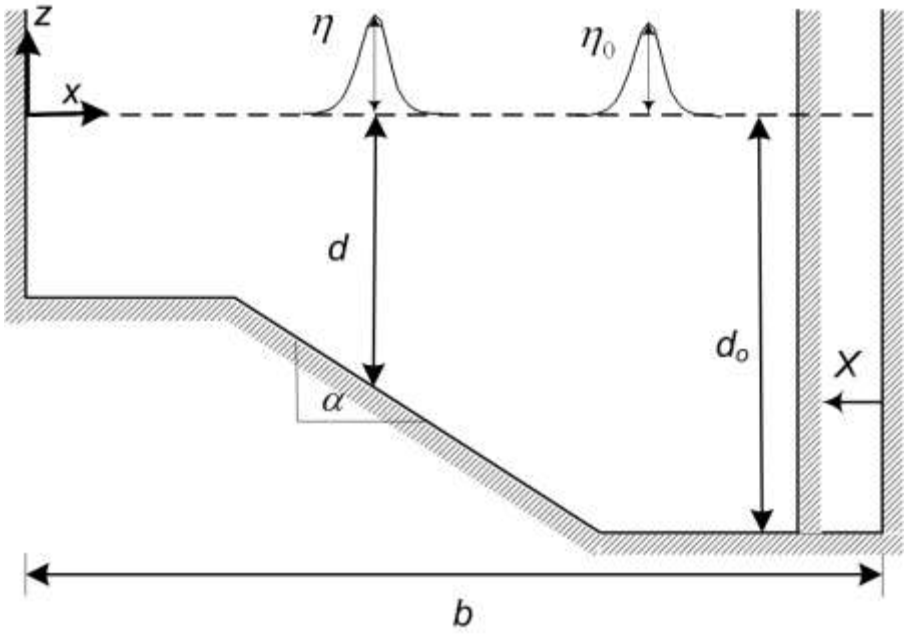

Fig. 8 Definition sketch of solitary wave passing over an inclined bed onto a shelf.

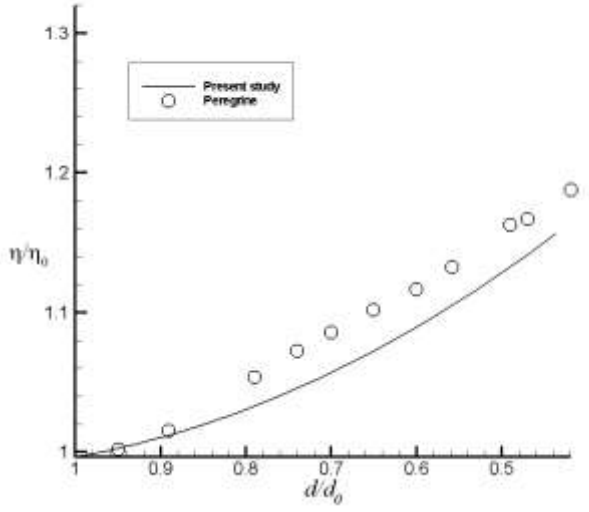

Fig. 9 Non-dimensional amplitude variation with depth, for beach slope=1/20 (solid line = present study; open circles = experimental data from Peregrine (1967)).